Particle swarm optimization technique for speed control and torque ripple minimization of switched reluctance motor using PID and FOPID controllers

M. Naveen Kumar[1] · R. Chidanandappa[1]

Abstract Switched Reluctance Motors has become one of the best solutions for EV applications because of its numerous benefits over other electric drive systems. Its excellent qualities are the robust design, double saliency, fault tolerance, and ability to withstand the heat of SRM drives. In order to minimize torque ripple and provide an exact speed response in SRM, this article mainly presents a speed and current control technique. The accurate speed control and torque ripple reduction of a SRM is controlled using the particle swarm optimization technique (PSO) with speed and current control mechanisms. The PID and FOPID speed controllers in the outer loop and current controller in the inner loop, respectively, are regulated, as are the 3-∅, 6/4 SRM turn-on (T_O), and turn-off (T_F), angles. The results were compared with existing optimization methods such as the SHO, LUS, GA, Ant-Lion, NSGA-II, MOLGSA, GSA, Hybrid MOLGSA, and RGA-SBX algorithms, show that a cascaded Fractional order PID(FOPID) controller offers better speed, current, and torque responses, as well as smaller current and torque ripples, under numerous different load and speed conditions. Under all load conditions, it has been demonstrated that the PSO-FOPID controller has the best speed response and minimal torque ripples when compared to the PSO-PID controller.

✉ M. Naveen Kumar
naveenkumar@nie.ac.in

R. Chidanandappa
chidananda@nie.ac.in

1 Electrical and Electronics Engineering Department, The National Institute of Engineering, Mysuru, Karnataka 570008, India

Abbreviation

PSO	Particle Swam optimization
ACO	Ant Colony optimization
GSA	Gravitational search algorithm
MOL	Many optimizations Liaison
ALO	Ant-Lion optimization
NSGA-II	Non-dominated sorting genetic algorithm
RGA-SBX	Real coded genetic algorithm simulated binary cross over
SHO	Spotted hyena optimizer
LUS	Local unimodal sampling
PID	Proportional-integral derivative
FOPID	Fractional order PID
GA	Genetic algorithm
SRM	Switched reluctance Motor
TSF	Torque Sharing Function
DTC	Direct Torque Control
ATC	Average Torque Control
ISE Speed	Integral squared error of speed
ISE Current	Integral squared error of current
FF	Fitness Function
T_O	Turn-on angle
T_F	Turn-off angle
μ	Derivative order
λ	Integral order
K_{ds}, K_{di}	Derivative gains of Cascaded controller
K_{is}, K_{ii}	Integral gains of cascaded controller
K_{ps}, K_{pi}	Proportional gains of cascaded controller
R_s	Per phase resistance
λ	Per phase flux linkage

Springer

V	Per Phase Voltage
e	Induced Electromotive force(emf)
K_b	Emf constant
L	Inductance
P_i	Instantaneous input power
i_s	Instantaneous DC current
ω_m	Rotor speed (rad sec)
$\varnothing$	Rotor position (rad)
P_a	Air gap Power
P	Differential operator
t	Time
T_e	Electromagnetic Torque
e_ω	Speed error in per unit
$\omega_{refp.u}$	Reference speed in per unit i.e., is 1 p.u
$\omega_{actp.u}$	Actual speed in per unit

1 Introduction

SRM is an effective competitor to BLDC, PMSM, and induction motors because of its inexpensive cost, simple construction, broad speed range, high torque when starting, flexible control, and fault tolerance [1]. In the last decade, researchers have carried out substantial studies on the SR Motor [2]. In Electric vehicle application SR Motors performance is good compared to induction motor, PMSM and BLDC motors [3]. SR Motor design has been greatly improved because of advanced development of power electronics converters and control techniques [4]. Due to their widespread usage in several applications including electric cars, robotic control applications, textile machines, and the aviation industries SR motors can run at high speeds [5]. Due to its double salient nature, continual switching action, and stator power supply, Nonlinear magnetic characteristics, undesirable torque ripples, and acoustic noise are typical problems with SR motors [6]. Because of these drawbacks, SR motors have a major influence on the system's reliability and safety. Researchers have also concentrated on developing novel control and design methodologies to enhance the performance of the SR Motor because standard regulation is challenging to implement properly [7]. The TSF, DTC, feedback control, and ATC techniques were described [8–11] to control torque ripples in SR Motor drives. The accurate speed response and torque ripple reduction of SRM utilizing LUS and SHO algorithms with PID and FOPID controllers were proposed in [12]. The author also discussed and compared with already existing optimization techniques with proposed techniques. Author mainly concentrated on torque ripples, speed response of SRM. Here main drawback of this study is constant T_O and T_F angles considered. utilizing current and speed control A method for reducing torque ripple was reported in [13] using a hybrid MOLGSA, MOL, and GSA with a PI controller and varying T_O and T_F angles.

For the purpose of controlling SRM drive speed and reducing torque ripple, [14] presented the Ant-Lion optimizer approach using a FOPID controller. The author also contrasted the recommended strategy with alternative optimisation techniques. In this scenario, it is assumed that the T_O and T_F are both constant. In [15], it was suggested to include a fuzzy logic controller to regulate an SRM's speed together with the accurate change of the T_O and T_F. in [16] focused on SRM torque ripple reduction utilizing a modified particle swarm optimization approach. in order to manage the speed of an SRM, [17] suggested using GA and an ant colony optimizer PID controller. The author focused mostly on PID speed control with optimization methods. The author did not examine the objective function in this case. The PSO technique is used to optimize a PID controller for SRM speed control [18]. The author mainly focused on speed control. The settling period of speed is lengthy here. The torque ripple reduction of SRM is described in [19] utilizing an artificial Bee colony optimization technique with a PID controller. The research's objective function is undefined. in [20] presents standard SRM motors and converter topologies, as well as various control approaches for minimizing torque ripples and SRM speed control. A unique objective function for double indicator optimisation is presented in [21]. In [22] offers a novel TSF implementation and an intelligent controller based on the flower pollination method for minimizing torque ripples in an SRM. The speed control of SRM using the ACO algorithm is described in [23]. In order to control PI, ACO is utilised. Here, a supply is provided by a photovoltaic system. A universal torque controller is described in [24] to eliminate torque ripple, increase the torque/current ratio, and enhance motor efficiency. The 8/6 SR motor is described in [25]. The toothed design of the rotor causes the SRM to vibrate and create acoustic noise. To overcome this problem, intelligent control systems such as ANN and FOPID have been created. [26] suggested a PEM fuel cell stack-feeding SRM using a multi-objective dragonfly optimizer. The author concentrated on three important performance indicators: torque per ampere ratio, torque smoothness factor, and average starting torque. [27] describes how to regulate SRM speed with torque ripple minimization using the NSGA-II algorithm. The PI controller is utilized here. In this method objective function is not clear. In SRM [28], turn-off angle variation using fuzzy logic is shown to reduce torque ripple. In [29], MOL techniques for controlling speed and reducing SRM torque ripple were introduced. in [30] presents a PID controller-based speed control of SRM with constant T_O and T_F. here, the settling time of speed response is very slow. Using Artificial neural network torque ripple and speed control of SRM with constant T_O and T_F presented in [31]. Speed control and performance indices of DC Motor is presented using PID controller [32, 33]. As seen in the previous literature, SRM

speed control and torque ripple reduction are presented with specific speed and load torque, but in this proposed work, the performance of SRM is presented under different speed and loading conditions, and the results are analysed and compared with the proposed optimisation technique with already exciting optimisation techniques. Therefore, main contribution of this article.

1. Developing a cascaded PID and FOPID controller that improves the speed response of a 6/4 pole SR motor in addition to minimizing torque ripples and which enables accurate speed control.
2. Implementing the particle swarm optimization (PSO) technique, design the optimum gains of the two cascaded PID and FOPID controllers.
3. Comparing the speed response and load torque at different conditions using already existing optimization technique with proposed model.
4. Checking the outcomes of the proposed PSO-PID and PSO-FOPID controllers with those described in earlier literature.

The work is divided into five sections: Sect. 1 has an introduction, Sect. 2 contains the mathematical model of the SR Motor, and Sect. 3 contains a case study, the formulation of the objective function, and a description of the recommended optimization techniques. Sections 4 and 5 present the results and Discussions. Finally, Sect 6 discussed conclusions.

2 Mathematical modelling of SR Motor

Figure 1 illustrates the 1-ϕ equivalent circuit model of SRM drive.

The resistive voltage drops and the rate of change of flux linkages are added together to form the applied voltage to a phase in SRM is given in below.
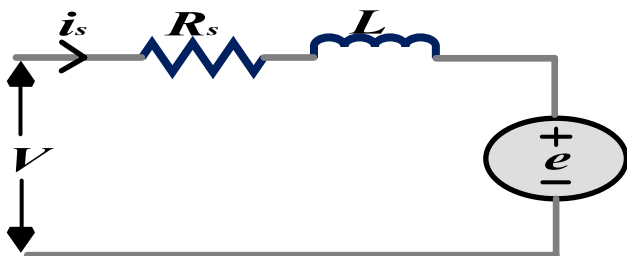

Fig. 1 Single phase equivalent circuit of SRM

$$V = R_s i + \frac{d\varphi(\theta, i)}{dt} \tag{1}$$

where, R_s= per-phase resistance, φ= per-phase flux linkage
Equation of φ given by:

$$\varphi = L(\theta, i).i \tag{2}$$

where, L is the inductance depends upon on the rotor position as well as the phase current (I_{Phase}).
Then, Phase voltage equation is

$$V = R_s i + \frac{d\{L(\theta, i)i\}}{dt} = R_s i + L(\theta, i)\frac{di}{dt} + i\frac{d\theta}{dt}.\frac{dL(\theta, i)}{d\theta}$$

$$V = R_s i + L(\theta, i)\frac{di}{dt} + \frac{dL(\theta, i)}{d\theta}\omega_m i \tag{3}$$

The induced Electromotive force(emf) equation is given below as:

$$e = \frac{dL(\theta, i)}{d\theta}\omega_m i = K_b \omega_m i \tag{4}$$

$$K_b = \frac{dL(\theta, i)}{d\theta} \tag{5}$$

The input power of SRM is given by

$$P_i = V.i$$

$$P_i = R_s i^2 + i^2 \frac{dL}{dt}(\theta, i) + L(\theta, i)i\frac{di}{dt} \tag{6}$$

$$\frac{d}{dt}\left(\frac{1}{2}L(\theta, i)i^2\right) = L(\theta, i)i\frac{di}{dt} + \frac{1}{2}i^2\frac{dL(\theta, i)}{dt} \tag{7}$$

Equation (7) and (6) form an Eq. 8 shown below

$$P_i = R_s i^2 + \frac{d}{dt}\left(\frac{1}{2}L(\theta, i)i^2\right) + \frac{1}{2}i^2\frac{dL(\theta, i)}{dt} \tag{8}$$

$$time(t) = \frac{\theta}{\omega_m} \tag{9}$$

Air gap power equation is

$$P_a = \frac{1}{2}i^2\frac{dL(\theta, i)}{dt} = \frac{1}{2}i^2\frac{dL(\theta, i)}{d\phi}.\frac{d\theta}{dt} = \frac{1}{2}i^2\frac{dL(\theta, i)}{d\theta}\omega_m \tag{10}$$

$$P_a = \omega_m T_e \tag{11}$$

From Eq. 10 and 11 we will get Eq. 12 shown below

$$T_e = \frac{1}{2}i^2\frac{dL(\theta, i)}{d\theta} \tag{12}$$

1188

Int. j. inf. tecnol. (February 2024) 16(2):1185–1201

3 Case study

Figures 7 & 8 illustrates the simulation model, a 6/4, 3-$\varnothing$ SRM with a total output power of 60KW [12]. The SRM is powered by a 3-$\varnothing$ asymmetrical converter with a 240 V dc supply. A position sensor is attached to the rotor with optimized T_O and T_F values to regulate the switching frequency of phase currents. The SRM model is simulated in MATLAB/Simulink using the requirements stated in the appendix. A cascaded PID and FOPID controller with reference speeds of 1000 rpm, 1500 rpm, and 2000 rpm are incorporated to provide speed and current control in the outer & inner loops respectively.

3.1 Minimization of torque ripple in SRM drive

The Change in machine co-energy i.e., high torque ripple was caused by the position of a rotor, flux linkage of a stator, and excitation current. The inductance was affected by these factors were strongly reliant with nonlinear position of a rotor, which causes variation in phase current. By balancing the current profile and choosing suitable T_O and T_F, the torque ripple may be reduced. In this work, T_O and T_F control is proposed together with torque ripple reduction for controlling current and speed. The speed controller and current controller employ standard PID and FOPID controller models. To improve the efficacy of the SRM drive, suitable combinations of eight optimal parameters for PID and twelve optimal parameters for FOPID have been identified, respectively. By using PSO optimization algorithm we will tune the PID and FOPID controller parameters these are Proportional, integral, derivative gains and Lambda(λ) and μ for both speed & current controllers and T_O & T_F angles. The optimal combination of these gain values can enhance the performance of the SRM drive and torque ripples. In this situation, FOPID will perform better than a PID controller. The ISE Speed and ISE Current are two common forms of integral square errors which were used to assess the errors of speed & current respectively, as shown below Eqs. (14) and (15).

$$f = ISE = \int_0^\infty e_\omega^2 dt \tag{13}$$

$$ISE\_Speed = \int (w_{ref} - w_m)^2 dt \tag{14}$$

$$ISE\_Current = \int (I_{ref} - I_m)^2 dt \tag{15}$$

Below Eq. 16 shown the torque ripple coefficient [27]

$$T_{ripple} = \frac{T_{max} - T_{min}}{T_{mean}} \tag{16}$$

The following torque equation can be used to characterize the SRM performance [34].

$$T_{Phase}(\theta, i) = \frac{1}{2} i^2 \frac{dL(\theta, i)}{d\theta} \tag{17}$$

where [13] T_{phase} is computed by the parameters using L, θ, i, and $T_{total}(\theta, i)$ (the total torque generated by 3-$\varnothing$ current) defined in the Eq. (18):

$$T_{total}(\theta, i) = \sum_{phase} \frac{1}{2} i^2 \frac{dL(\theta, i)}{d\theta} \tag{18}$$

The proposed optimization algorithm and objective function are described in the next section, and Fig. 2a, b, and c shows the variations in the 3-$\varnothing$ flux, current, & characteristics of magnetization.

3.2 Problem formulation

The inner current controller and outer speed controller are the two PID and two FOPID controllers that will be optimized in this scenario will enhance the response of speed & reduce the disturbances in the working functions of SRM. In order to make this efficient, Eqs. (19) and (20) are used to create the proposed FF, it is the summation of ISE current & speed [17].

The constraints considered in the formulation of the multi-objective problem are the ISE current of the inner loop and the ISE speed of the outer loop. The following two objectives are mentioned below.

As seen below, the minimization of the ISE current & speed is described by Eqs. (19) and (20).

$$f_1 = \min(ISE_{speed}) \tag{19}$$
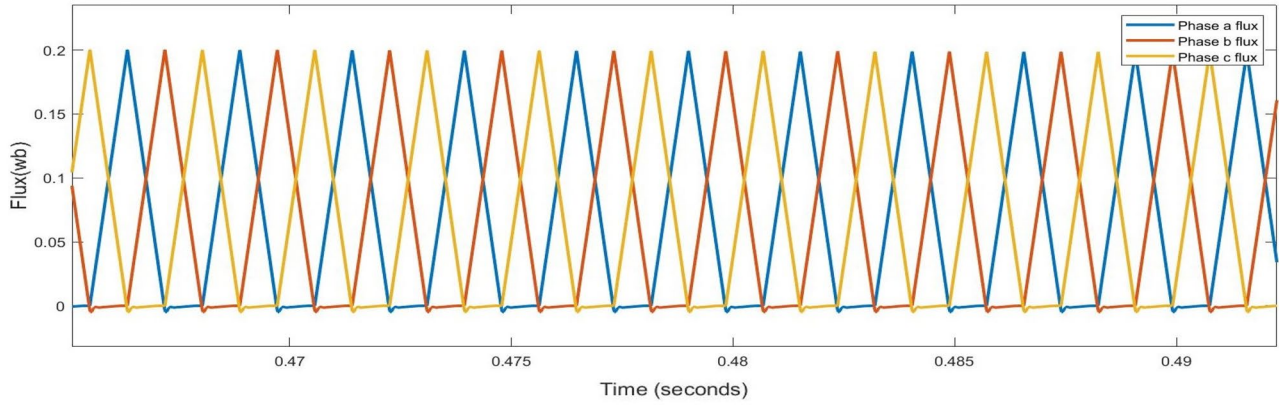
$$f_2 = \min(ISE_{current}) \tag{20}$$

This is a method to formulate the optimization problem given below in Eq. (21)

$$Minf = \left(\int_0^{t_{sim}} (w_{ref} - w_m)^2 dt \right) + \left(\int_0^{t_{sim}} (I_{ref} - I_m)^2 dt \right) \tag{21}$$
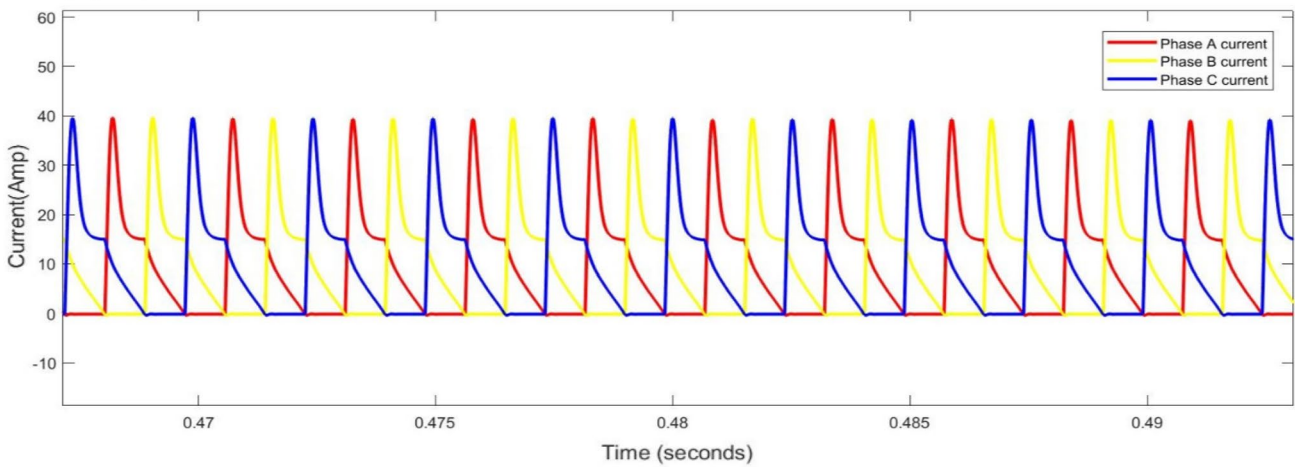
$$minf = f_1 + f_2 \tag{22}$$

the following constraints are also subjected to the objective function:

(a) 3-∅ flux

(b) 3-∅ current

(c)
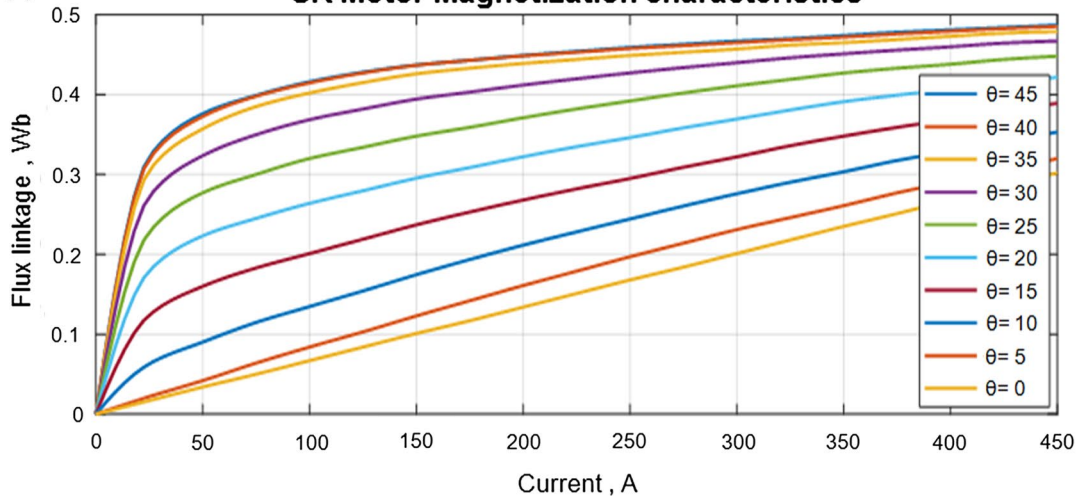
Fig. 2 **a** Three phase flux **b** three phase current **c** characteristics of magnetization

1190
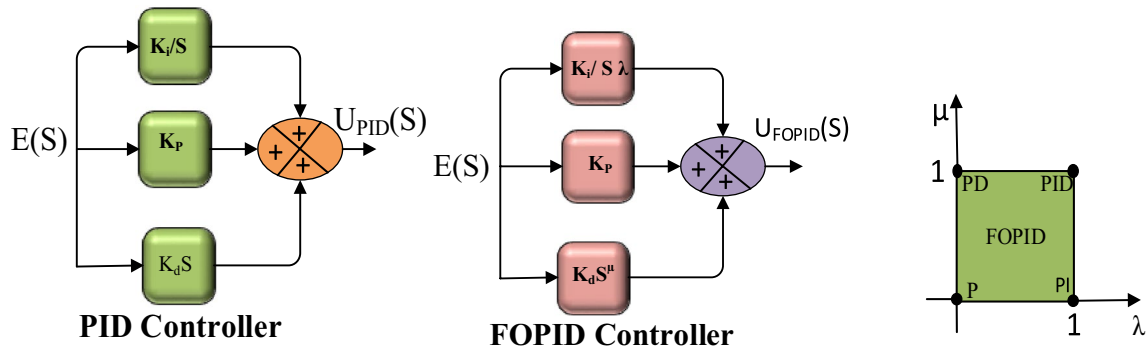
Int. j. inf. tecnol. (February 2024) 16(2):1185–1201

Fig. 3 Block diagram of PID, FOPID and time domain of FOPID controller

$K_{p1,min} \leq K_{p1} \leq K_{p1,max}$

$K_{i1,min} \leq K_{i1} \leq K_{i1,max}$

$K_{d1,min} \leq K_{d1} \leq K_{d1,max}$

$K_{p2,min} \leq K_{p2} \leq K_{p2,max}$

$K_{i2,min} \leq K_{i2} \leq K_{i2,max}$

$K_{d2,min} \leq K_{d2} \leq K_{d2,max}$

$K_{p1,min} \leq K_{p1} \leq K_{p1,max}$

$K_{i1,min} \leq K_{i1} \leq K_{i1,max}$

$\lambda_{min} \leq \lambda_1 \leq \lambda_{max}$
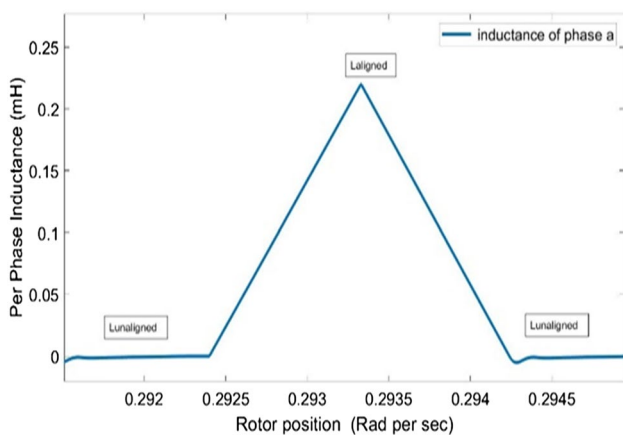
$K_{d1,min} \leq K_{d1} \leq K_{d1,max}$

$\mu_{min} \leq \mu_1 \leq \mu_{max}$

$K_{p2,min} \leq K_{p2} \leq K_{p2,max}$

$K_{i2,min} \leq K_{i2} \leq K_{i2,max}$

$\lambda_{min} \leq \lambda_2 \leq \lambda_{max}$

$K_{d2,min} \leq K_{d2} \leq K_{d2,max}$

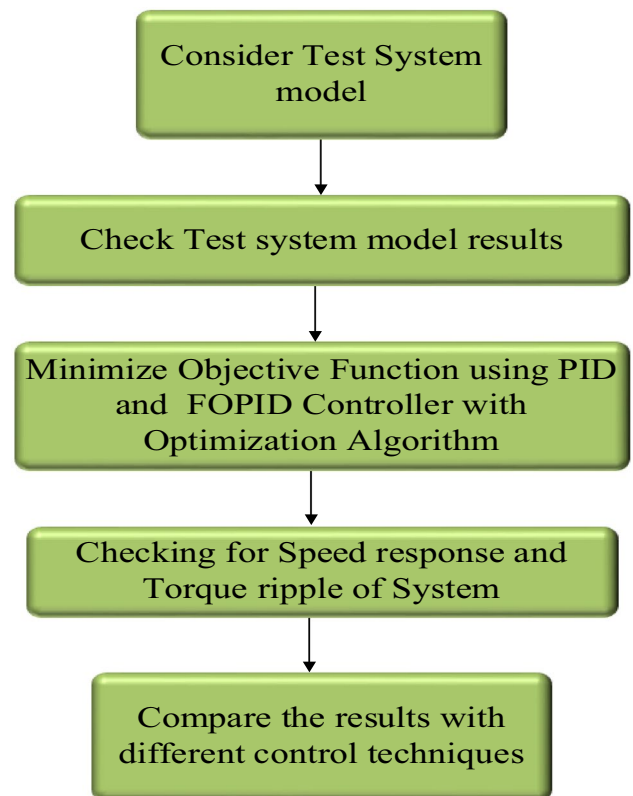**Fig. 4** Rotor position vs per phase inductance
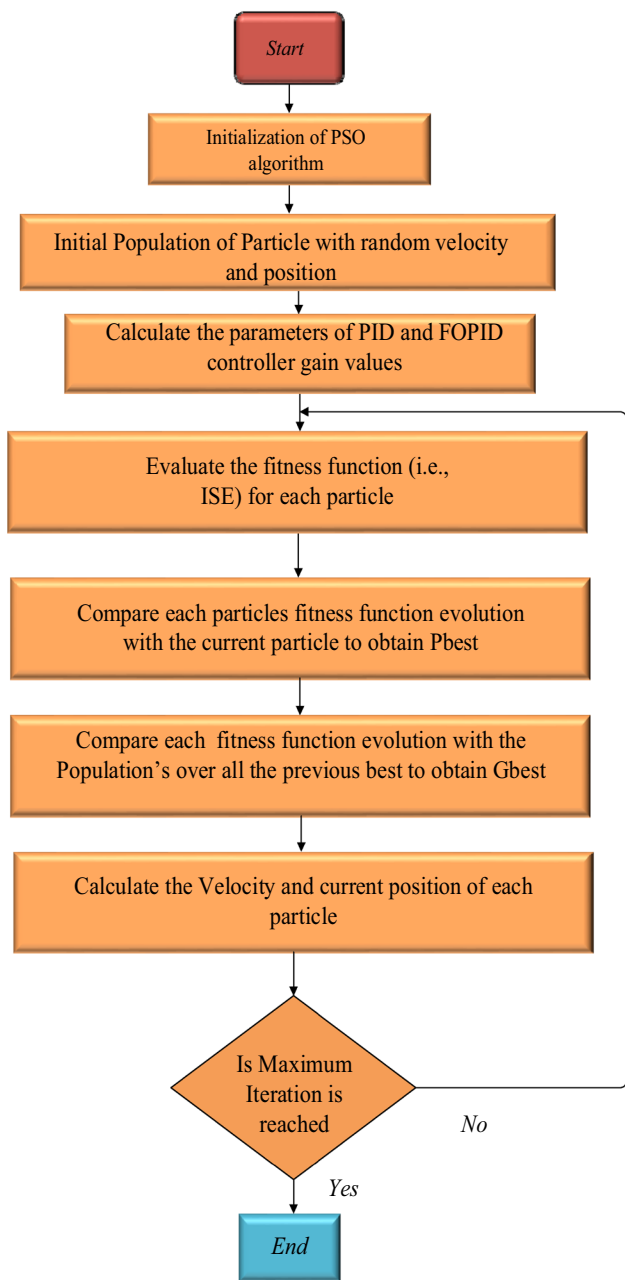

Fig. 5 Flowchart for proposed system

Fig. 6 Flowchart of PSO algorithm

$$\mu_{min} \leq \mu_2 \leq \mu_{max}$$

where K_{p1}, K_{i1}, K_{d1} and K_{p2}, K_{i2}, K_{d2} are the PID speed and current controller gains and $K_{p1}, K_{i1}, \lambda_1, K_{d1}, \mu_1$ and $K_{p2}, K_{i2}, \lambda_2, K_{d2}, \mu_2$ are the FOPID speed and current controller gains respectively.

The upper and lower limits for each PID, FOPID speed, and current parameter are provided in Eqs. (23) and (24), (25), and (26) respectively.

$$K_{ps} \in [0, 10], K_{is} \in [0, 10] \, and \, K_{ds} \in [0, 10] \tag{23}$$

$$K_{pi} \in [0, 10], K_{ii} \in [0, 10] \, and \, K_{di} \in [0, 10] \tag{24}$$

$$K_{ps} \in [0, 10], K_{is} \in [0, 10], \lambda_{is} \in [0, 1], K_{ds} \in [0, 10] \, and \, \mu_{is} \in [0, 1] \tag{25}$$

$$K_{pi} \in [0, 10], K_{ii} \in [0, 10], \lambda_{ii} \in [0, 1], K_{di} \in [0, 10] \, and \, \mu_{ii} \in [0, 1] \tag{26}$$

θ_{on} and θ_{off} of lower and upper bounds are shown below equations,

$$\theta_{on} \in [38.5, 51.5] \tag{27}$$

$$\theta_{off} \in [60, 90] \tag{28}$$

3.3 Brief description of PID and FOPID controller

Due to its simple form and ease of parameter adjustment, a PID controller is the most extensively used controller in the industry for control applications. A traditional PID control approach does not deliver adequate performance when the process gets too complicated to define. As a result, it is incapable of capturing all design objectives and requirements over a wide variety of operating circumstances and disturbances [35].

$$G_c(S) = K_p + K_i \frac{1}{S} + K_D S \tag{29}$$

For these reasons, FOPID controller configurations have been provided in multiple studies under various operating circumstances of the controlled systems to achieve the lowest steady-state error and enhance dynamic behaviour.

In recent years, academia and business have shown a strong interest in the FOPID controller [36]. actuality, because they have five parameters to choose from rather than three, they provide greater flexibility in controller design than a standard PID controller [37]. This, however, suggests that controller tuning may be far more complex. Figure 3 illustrates the PID, FOPID, and time domain of the FOPID controller block diagram. A fractional order PID controller's most popular design is the $PI^\lambda D^\mu$ controller involving an integrator of order λ and a differentiator of order μ.

where λ and μ can be any real numbers. The transfer function of Such a controller has the form

$$G_c(S) = K_p + K_i \frac{1}{S^\lambda} + K_D S^\mu, (\lambda, \mu) > 0 \tag{30}$$
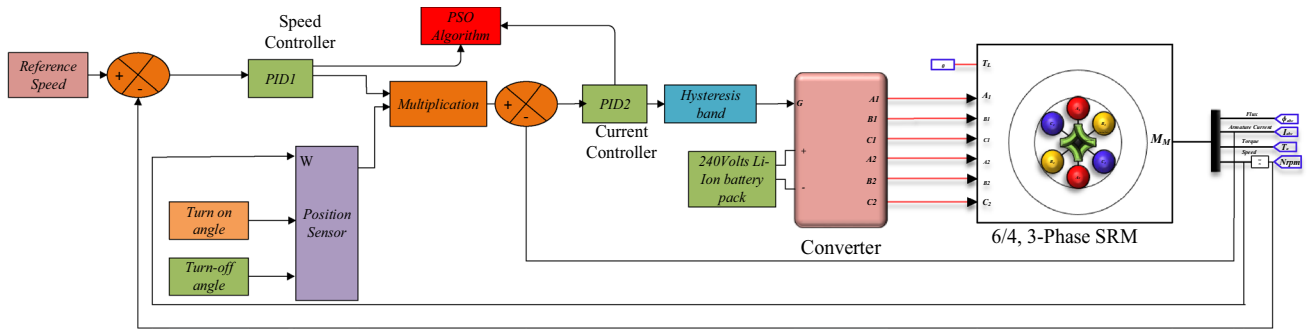
1192

Int. j. inf. tecnol. (February 2024) 16(2):1185–1201

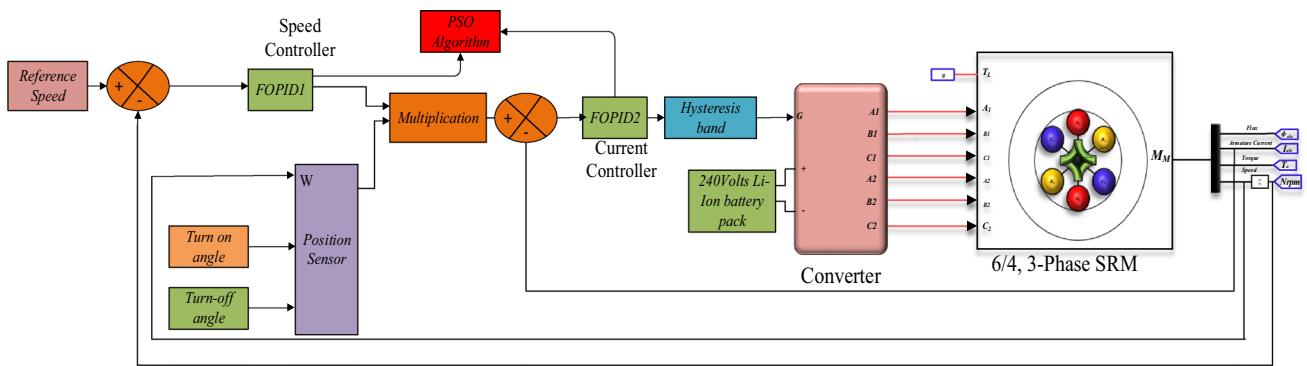**Fig. 7** Simulation model of SRM with PSO-PID Controller

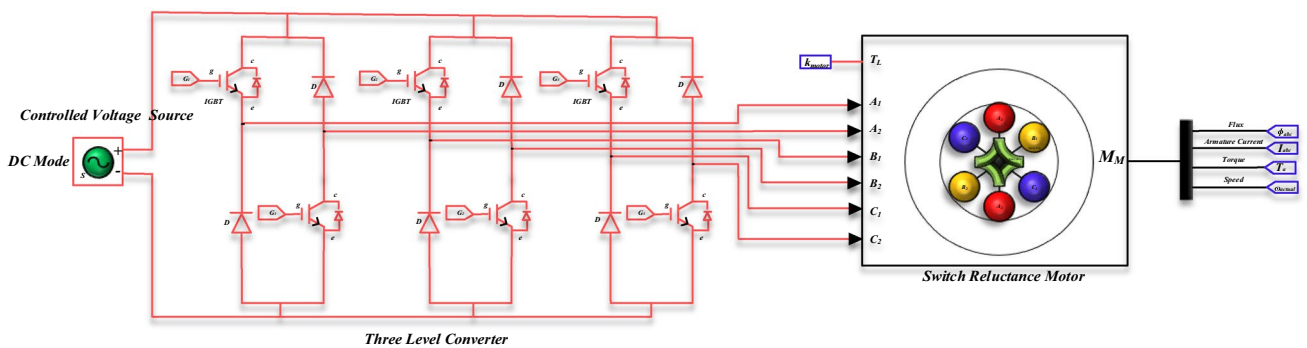**Fig. 8** Simulation model of SRM with PSO-FOPID Controller

Fig. 9 Three level asymmetric converter model to drive SRM motor

3.4 Turn-on and turn-off angle design

The T_O and T_F ultimately decide how well SRM performs. A number of variables which includes torque ripple, acoustic noise, torque-speed range and machine efficiency are influenced by T_O and T_F. Figure 4 depicts the stator's per-phase inductance curve with rotor position advancement in Radians per second.

T_O: Rotor angle at the instant when respective phase is excited.

T_F: Rotor angle at the instant when conducting phase turned off.

3.5 Methodology

Figure 5 shows the steps to find the Speed control and Torque ripple minimization of SRM drive.

Table 1 Output Results when ISE is optimized using PSO-FOPID

(Nm)	N (rpm)	θ°_{on}	θ°_{off}	K_{ps}	K_{is}	K_{ds}	λ	μ	K_{pi}	K_{ii}	K_{di}	λ	μ	T_{max}	T_{min}	T_{mean}	T_{ripple}
0	1000	47.3149	73.043	1.498	0.2633	0.2848	0.4958	0.1882	5.7156	4.205	0.879	4.516	0.824	2.21	1.913	2.066	0.14811
	1500	41.7797	69.735	3.649	2.1332	1.8103	0.9054	0	6.0365	3.077	7.970	0.745	0.436	3.11	1.782	2.320	0.57370
	2000	49.9438	72.825	7.612	0.3211	1.8538	0.4001	0	3.8361	2.948	3.901	0.843	0.614	4.16	2.3157	3.4236	0.5409
25	1000	46.7065	75.276	2.505	4.3581	0.0812	0.6565	0.738	7.4555	6.528	4.849	0.662	0.539	27.1	25.04	26.13	0.08
	1500	45.5339	71.224	3.844	5.5961	0	1	1	7.2268	3.751	4.4730	0.18584	0.385	29.6	27.78	28.50	0.063
	2000	44.4921	73.782	10	0	0	0.3423	0.5001	8.5990	0	0	1	1	28.2	25.63	26.69	0.097
50	1000	45.0758	87.295	3.477	7.8987	0.7476	0.7239	0.212	6.0427	5.336	0	0.602	0.4728	53.5	46.63	50.56	0.135
	1500	47.3491	77.365	3.623	4.8655	0.5214	0.6201	0.1376	7.36358	5.325	2.892	1	0.629	55.8	50.52	53.13	0.1010
	2000	43.0018	90	10	4.3160	3.7639	1	0	10	3.193	3.961	0.970	0.001	52.1	51.24	51.64	0.017
75	1000	46.6541	89.032	2.943	10	0	0.8242	0	4.8823	5.255	6.054	0.418	0.362	78.5	67.1	72.51	0.157
	1500	41.6861	88.088	4.387	7.1377	2.4553	0.9360	0	5.6576	3.169	0.162	0.248	0.819	79,5	74.41	74.48	0.069
	2000	43.9999	73.666	6.610	6.4901	0	0.9384	0.015	9.3120	4.688	1.301	0.103	0.579	78.41	71.82	74.48	0.088
100	1000	46.6541	89.032	2.943	10	0	0.82424	0	4.88237	5.255	6.054	0.418	0.362	98.8	94.81	96.94	0.042
	1500	40.0538	89.805	5.247	8.6067	0.0454	0.9334	0	7.8675	6.549	0.409	0.758	0.450	106	88.95	98.94	0.178
	2000	42.5052	73.877	5.036	8.2354	3.1254	0.9240	0	9.8948	7.040	0.176	0	0.235	108	104.6	106.6	0.039

Table 2 Output Results when ISE is optimized using PSO-PID

T_L (Nm)	N (rpm)	θ°_{on}	θ°_{off}	K_{ps}	K_{is}	K_{ds}	K_{pi}	K_{ii}	K_{di}	T_{max}	T_{min}	T_{mean}	T_{ripple}
0	1000	53	78	10	2.1662	0	9.8646	10	10	9.674	6.590	8.758	0.352
	1500	48	79.6354	10	4.0565	0	8.9869	0	0.3289	3.21	3.131	3.17	0.02
	2000	48	79.6673	10	0	0	10	1.5653	10	6.421	5.844	6.133	0.094
25	1000	48.526	81	10	8.5298	0	3.5030	4.7352	0.4879	27.96	26.66	27.32	0.047
	1500	48	81	10	7.1167	0	7.29912	2.2131	0.1217	28.69	25.16	27.19	0.1298
	2000	48	78	10	2.9911	0	10	0.3839	0	27.94	22.71	25.16	0.207
50	1000	48	81	10	9.4554	0	6.5079	5.4676	0.3830	55.33	48.91	51.11	0.1256
	1500	48	78	10	9.2868	0	10	0	0.2681	56.64	49.50	52.39	0.1364
	2000	48	78.9683	10	4.1978	0	10	0.4529	0	48.90	44.24	46.64	0.0999
75	1000	48	78	10	10	0	10	10	2	77.45	75.25	76.41	0.013
	1500	48	80.99	10	8.0435	0	6.3956	0.9142	0.0907	98.40	63.82	78.37	0.4413
	2000	48	78	10	5.6435	0	10	0	0	78.81	77.98	78.41	0.01
100	1000	48.014	78	9.3932	8.9797	0	9.6687	9.2262	3.4673	136.7	60.45	103.3	0.7381
	1500	48.01	78.68	10	10	0	10	0	0.1193	133.1	76.55	104.29	0.542
	2000	48	78.7892	10	10	0	7.3126	0	0	115.2	94.59	101.2	0.203

1194

Int. j. inf. tecnol. (February 2024) 16(2):1185–1201

Table 3 Optimal FF using PID controller and different algorithms at 1000 rpm

Algorithm & Controller	Case 1 (T = 0 N.m.)	Case 2 (T = 50 N.m.)	Case 3 (T = 100 N.m.)
PSO-PID(Proposed)	2.22e + 03	2.296e + 03	2.385e + 03
RGA-SBX-PI [27]	7.345e + 04	4.833e + 03	2.745e + 03
NSGA-II-PI [27]	1.556e + 04	8.390e + 03	3.916e + 03
Hybrid MOLSA-PI [13]	4.703e + 03	5.129e + 03	4.182e + 03
MOL-PI [13]	4.709e + 3	1.005e + 04	4.270e + 03
GSA-PI [13]	4.787e + 03	4.127e + 03	4.316e + 03
LUS-PID [12]	9.913e + 03	2.700e + 03	2.856e + 03
SHO-PID [12]	3.626e + 03	2.317e + 03	2.405e = 03

Table 4 Optimal FF using PID controller and different algorithms at 1500 rpm

Algorithm & Controller	Case 1 (T = 0 N.m.)	Case 2 (T = 50 N.m.)	Case 3 (T = 100 N.m.)
PSO-PID(Proposed)	5.832e + 03	5.999e + 03	6.156e + 03
RGA-SBX-PI [27]	2.33e + 04	6.988e + 03	6.361e + 03
NSGA-II-PI [27]	5.906e + 04	9.199e + 03	7.436e + 03
Hybrid MOLSA-PI [13]	1.308e + 04	1.44e + 04	3.13e + 04
MOL-PI [13]	8.609e + 04	1.055e + 04	7.953e + 03
GSA-PI [13]	2.019e + 04	1.256e + 04	6.267e + 03
LUS-PID [12]	6.853e + 03	7.308e + 03	7.889e + 03
SHO-PID [12]	6.121e + 03	6.019e + 03	6.353e + 03

Table 5 Optimal FF using PID controller and different algorithms at 2000 rpm

Algorithm & Controller	Case 1 (T = 0 N.m.)	Case 2 (T = 50 N.m.)	Case 3 (T = 100 N.m.)
PSO-PID(Proposed)	1.147e + 04	1.183e + 04	1.211e + 04
RGA-SBX-PI [27]	1.158e + 04	1.184e + 04	1.222e + 04
NSGA-II-PI [27]	1.157e + 04	1.189e + 04	1.234e + 04
Hybrid MOLSA-PI[13]	1.152e + 04	1.186e + 04	1.208e + 04
MOL-PI [13]	1.154e + 04	1.190e + 04	1.211e + 04
GSA-PI [13]	1.158e + 04	1.192e + 04	1.216e + 04
LUS-PID [12]	1.457e + 04	1.538e + 04	1.742e + 04
SHO-PID [12]	1.172e + 04	1.208e + 04	1.251e + 04

Table 6 Optimal FF using FOPID controller and different algorithms at 1000 rpm

Algorithm & Controller	Case 1 (T = 0 N.m.)	Case 2 (T = 50 N.m.)	Case 3 (T = 100 N.m.)
PSO-FOPID(Proposed)	2.231e + 03	2.38156e + 03	2.387e + 03
GA-FOPID [14]	2.311e + 03	2.456e + 03	2.620e + 03
LUS-FOPID [12]	2.232e + 03	2.58815e + 03	2.728e + 03
SHO-FOPID [12]	5.049e + 03	2.836e + 03	2.638e + 03
Ant-lion-FOPID [14]	1.054e + 04	8.274e + 04	6.571e + 04

Table 7 Optimal FF using FOPID controller and different algorithms at 1500 rpm

Algorithm & Controller	Case 1 (T = 0 N.m.)	Case 2 (T = 50 N.m.)	Case 3 (T = 100 N.m.)
PSO-FOPID(Proposed)	5.821e + 03	5.988e + 03	6.138e + 03
GA-FOPID [14]	1.159e + 05	6.962e + 03	7.162e + 03
LUS-FOPID [12]	2.488e + 04	2.5065e + 04	7.227e + 03
SHO-FOPID [12]	6.615e + 03	6.970e + 03	7.633e + 03
Ant-lion-FOPID [14]	6.131e + 04	6.442e + 04	6.328e + 04

engineering problems that are challenging to solve using conventional optimization techniques. Kennedy and Eberhart created PSO in 1995. Research revealed that PSO performs better than other algorithms. It is a population-based stochastic search technique. One of the finest qualities of this method is its extremely straightforward algorithm. It only uses two equations, which makes it easier to understand. It also has a simple convergence characteristic and an acceptable computational approach. Figure 6 illustrates the flowchart of PSO algorithm.

Mathematically PSO can be explained as follows.

Velocity of particle (i) is adjusted as

$$V_j^{k+1} = WV_j^k + K_P \times R_p\left(P_{best_j} - X_j^k\right) + K_G \times R_G \times \left(G_{best}t - X_j^k\right) \tag{31}$$

Position of particle (i) is adjusted as

$$X_i^{k+1} = X_t^i + V_i^{k+1} \tag{32}$$

where, the position and velocity of jth particle at iteration k is represented by the variables V_j^k and X_j^k respectively. Shi and Eberhart described how to update the particle's velocity between iterations. The best position of swarm and agent j are G_{best} and P_{best_j} respectively. The cognitive and social parameters are predefined constants represented by K_P and K_G.

3.6 Brief description of PSO algorithm

Numerous heuristic optimization techniques, including the genetic algorithm (GA), ant colony algorithm (ACO), PSO, and most recently, biogeography-based optimization (BBO), have been developed recently to solve a variety of complex

Table 8 Optimal FF using FOPID controller and different algorithms at 2000 rpm

Algorithm & Controller	Case 1 (T = 0 N.m.)	Case 2 (T = 50 N.m.)	Case 3 (T = 100 N.m.)
PSO-FOPID(Proposed)	1.178e + 04	1.183e + 04	1.209e + 04
GA-FOPID [14]	1.373e + 04	1.46e + 04	1.571e + 04
LUS-FOPID [12]	1.416e + 04	1.597e + 04	1.7e + 04
SHO-FOPID [12]	1.802e + 04	2.009e + 04	2.367e + 4
Ant-lion-FOPID [14]	2.658e + 04	2.35e + 04	2.206e + 4
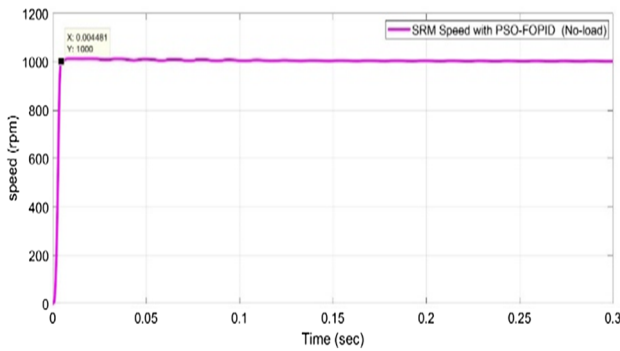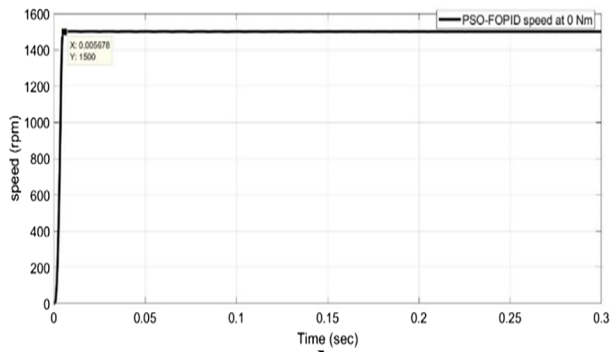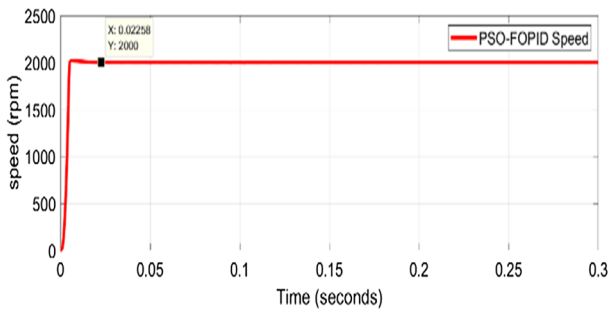
Fig. 10 PSO-FOPID No-Load Speed at **a** 1000 rpm, **b** 1500 rpm, **c** 2000 rpm
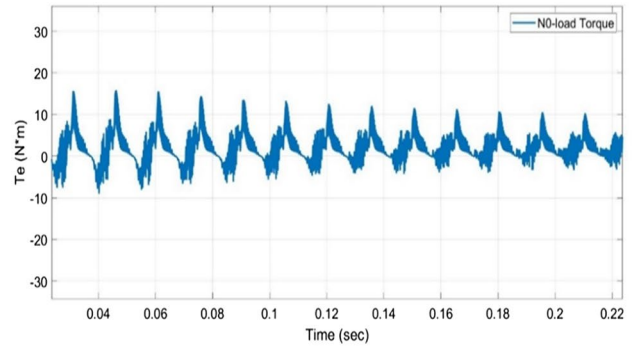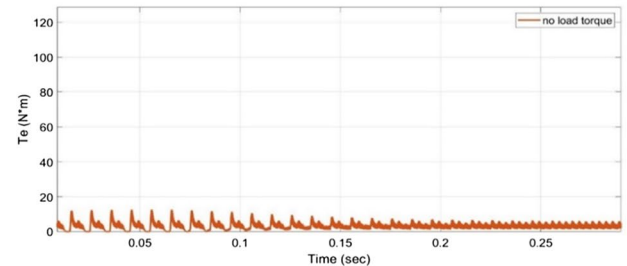

Fig. 11 PSO-FOPID No-Load torque at **a** 1000 rpm, **b** 1500 rpm, **c** 2000 rpm
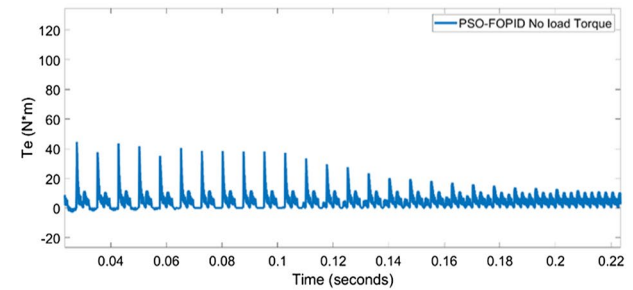
The random numbers between 0 and 1 that were created are R_p and R_G. In order for the PSO exploration process to find an optimal solution quickly and with fewer iterations, the inertia weight W keeps a balance between global and local search. The equation below shows that as the search process advances, the inertia weight W decreases linearly.

$$W = W_{max} - \left(\frac{W_{max} - W_{min}}{K_{max}} \right) K \tag{33}$$
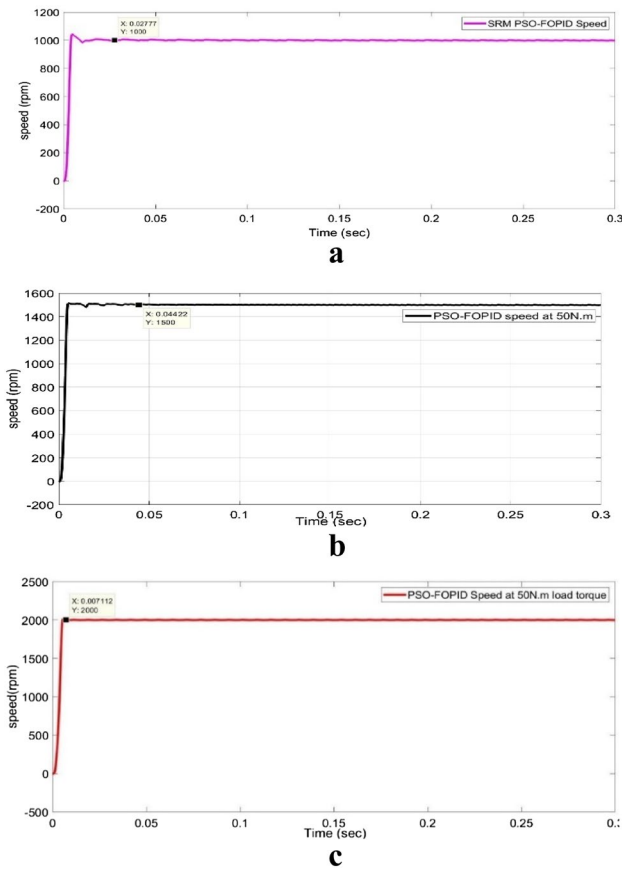
Fig. 12 PSO-FOPID (50 N.m. load) Speed at **a** 1000 rpm, b. 1500 rpm, **c** 2000 rpm

Here, W_{max} and W_{min} respectively, represent the inertia weight's maximum and minimum values.

4 Results and discussions

The proposed system for controlling speed and current consists of two controller loops. Figures 7 and 8 illustrates a three-phase SRM with a PID and FOPID speed controller in the outer loop and a PID and FOPID current controller in the inner loop, as well as an angle control for the T_O and T_F system. With the aim of simultaneously minimizing torque ripple and integral square error of speed and current, the multi-objective optimization problem statement is defined as searching the values of proportional, integral, and derivative gains, Lambda, and μ of PID and FOPID controllers for both current and speed controllers as well as T_O and T_F angle.

The particle swarm optimization (PSO) algorithm has been developed in. mfile and the model of the system under investigation has been developed in MATLAB/
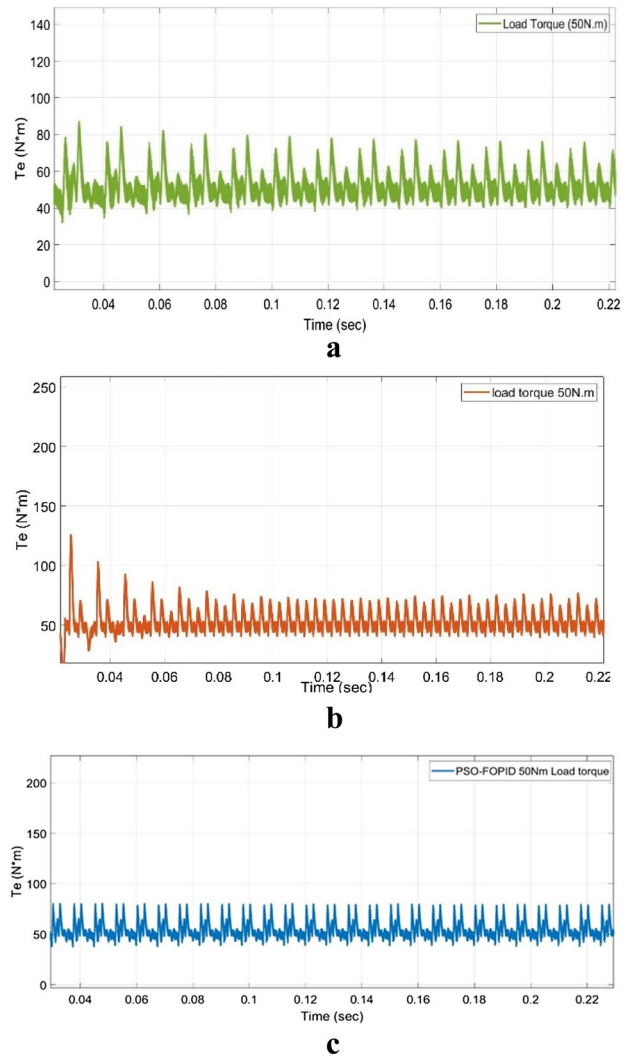
Fig. 13 PSO-FOPID 50N.m Load Torque at **a** 1000 rpm, **b** 1500 rpm, **c** 2000 rpm

SIMULINK environment. Figure 9 shows the three-level asymmetric converter model to drive SRM.

The analysis and simulation of three loading scenarios for 1000 rpm, 1500 rpm, 2000 rpm for various loading conditions these loading cases are: case 1: No load, case 2: 50N.m, case 3: 100N.m. load is simulated for 0.3 s interval.

Table 1 and 2 represent the current and speed controllers' PID and FOPID optimal gain values for the five loading conditions. Additionally, the results of various controllers developed in earlier literature and optimized using GA, Antlion, SHO, LUS, Ant colony, NSGA-II, MOL, RGA-SBX, GSA, and Hybrid MOLGSA are compared to the outcomes of the SRM time response with PID and FOPID coefficients optimized using PSO algorithms. Additionally, Table 3, 4, 5, 6, 7 and 8 provide the optimal FF values for the three
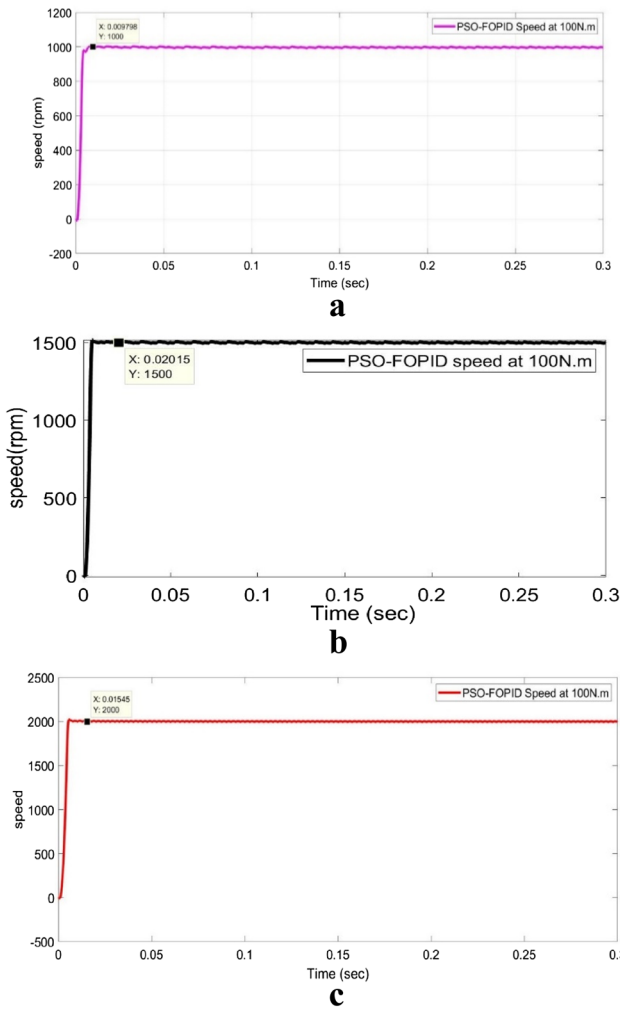
Fig. 14 PSO-FOPID (100 N.m. load) speed at **a** 1000 rpm, **b** 1500 rpm, **c** 2000 rpm

Fig. 15 PSO-FOPID (100 N.m. load) speed at **a** 1000 rpm, **b** 1500 rpm, **c** 2000 rpm

loading scenarios while using various controllers with different speeds. The FF values for the PSO-FOPID controller are the lowest when compared to those of other optimization techniques.

Case 1: no-Load torque (T = 0N.m). Figure 10 and 11 illustrate the outcomes of the simulation for this case. In comparison to other techniques, the PSO-FOPID algorithm offers a better speed response when applying a reference speed of 1000, 1500, or 2000 rpm. As seen in Fig. 10a, b, c, Due to its quick response time and minimal study state error, the PSO technique offers the best transient and study-state performance. The PSO algorithm performs slightly better than other Techniques in terms of speed. Unfortunately, the high settling time of the GA Technique results in low-speed performance. Various speed ranges of the no load torque are presented in Fig. 11a, b, c. It can be observed through a
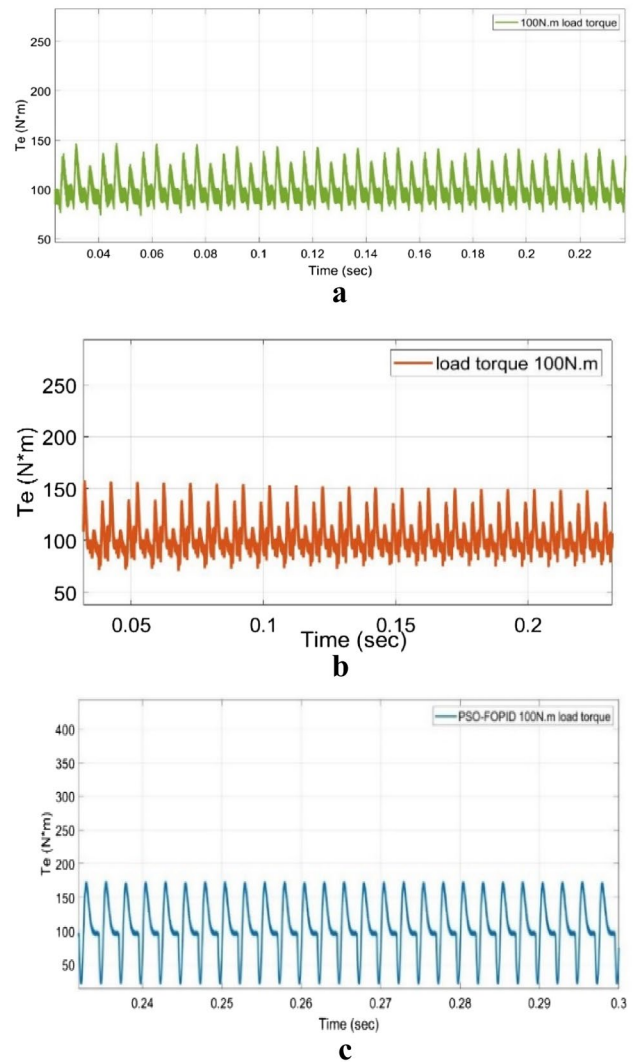
comparison of the PSO and GA that the PSO can generate the lowest current ripples.

Case 2 T = 50N.m. In this scenario, the SRM drive is subjected to a load torque of 50N.m at three different speeds (i.e., 1000, 1500, and 2000 rpm) at time t = 0.3 s shown in Fig. 12a, b, c. When compared to PSO-PID and GA, PSO-FOPID provides a faster speed response. Although the PSO-FOPID algorithm exhibits some allowable overshoot, it offers a quick response and is not impacted by disturbances. The Ant-colony, Ant-lion, and GA algorithms exhibit some study state error and slightly slower speed response compare to the PSO algorithm. The disturbance torque substantially affects the GA and has a worse off-speed response. The load torque under this case is shown in Fig. 13a, b, c from 0 to 0.3 s. The PSO
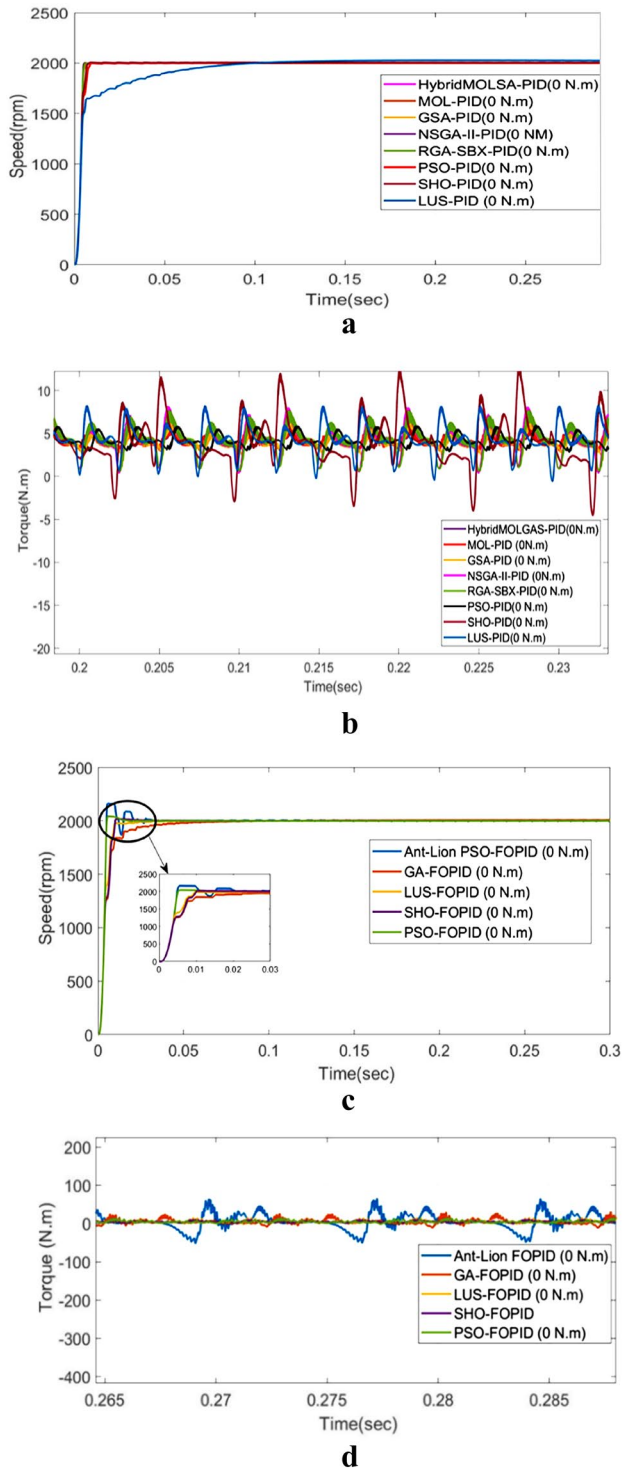
1198

Int. j. inf. tecnol. (February 2024) 16(2):1185–1201

Fig. 16 **a** PSO-PID speed at 2000 rpm, **b** PPSO-PID No-load torque at 2000 rpm, **c** PSO-FOPID speed at 2000 rpm, **d** PSO-FOPID No-load torque at 2000 rpm
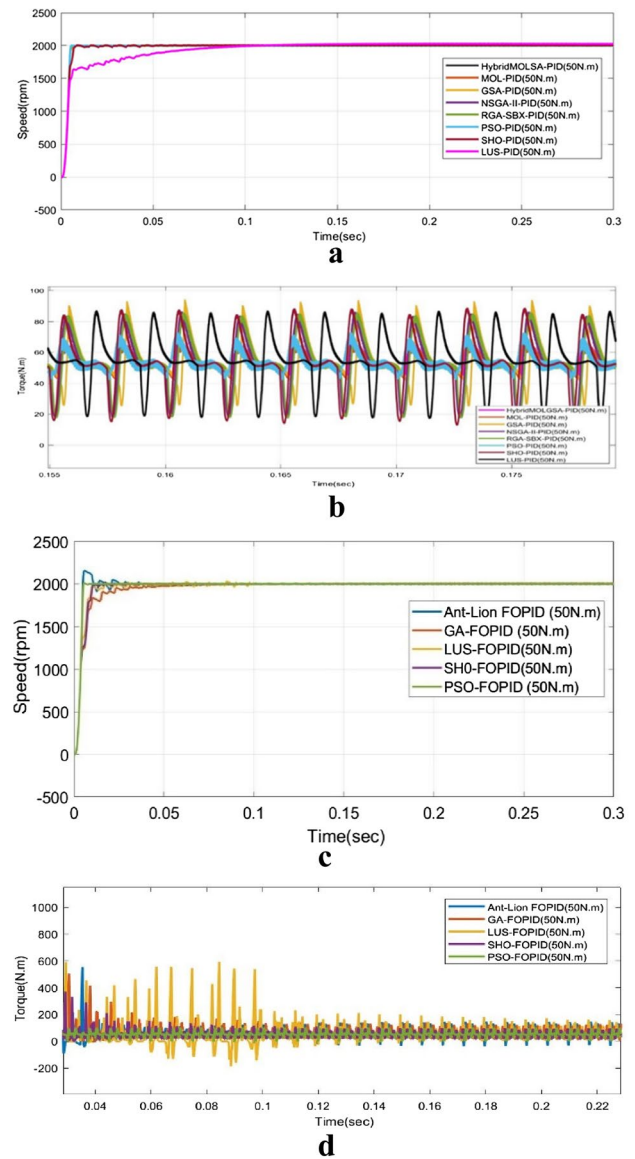

Fig. 17 **a** PSO-PID speed at 2000 rpm, **b** PSO-PID 50 N.m load Torque at 2000 rpm, **c** PSO-FOPID Speed at 2000 rpm, **d** PSO-FOPID 50 N.m load torque at 2000 rpm

technique produces the lowest torque ripples, whereas the GA algorithm produces larger torque ripples.

Case 3 T = 100N.m. Figures 14 and 15 display the simulation results for this scenario. In this case, the SRM drive is applied a load torque of 100N.m at three distinct speeds (i.e., 1000, 1500, and 2000 rpm). The outcomes of this case simulation results are depicted in figure below. the PSO-FOPID simulation analysis conducted for various speed responses.
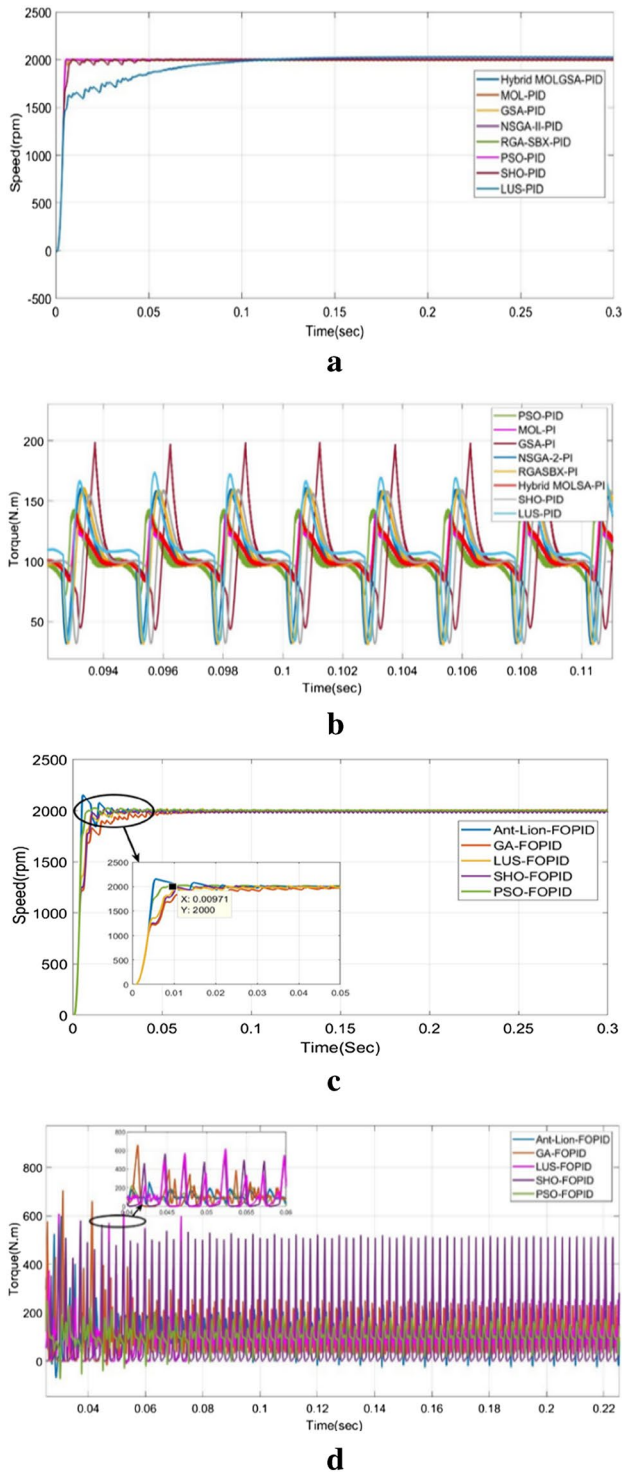
Fig. 18 **a** PSO-PID speed at 2000rpm, **b** PSO-PI D 100 N.m load torque at 2000 rpm, **c** PSO-FOPID speed at 2000 rpm, **d** PSO-FOPID 100 N.m load torque at 2000 rpm

the speed responses shown in Figs. 14a, b, c, 15a, b, c shows the PSO-FOPID load torque at 100N.m. at three distant speed ranges.

4.1 Comparison between PSO-FOPID controller with already existing algorithms

The effectiveness of the proposed PID and FOPID controllers using the PSO algorithm is compared in this section. As can be observed, PSO-FOPID has superior convergence and is more efficient than PSO-PID. Moreover, Tables 2 and 3 demonstrate optimal gains of PSO-PID, PSO-FOPID, and maximum, minimum, mean, and torque ripples for PSO-PID and PSO-FOPID controllers. When comparing the two techniques, PSO-FOPID produces less torque ripples than PSO-PID.

5 Discussions

Case 1: no load torque T = 0Nm. The PSO-FOPID's speed response setting time in Fig. 16c is considerably faster than Ant-lion-FOPID, SHO-FOPID, LUS-FOPID, GA-FOPID, respectively. As a result, The PSO-FOPID has the fastest speed response. In Fig. 16d shows the No-load torque at 2000 rpm speed, PSO-FOPID has very less torque ripples compare to Ant-lion-FOPID, SHO-FOPID, LUS-FOPID, GA-FOPID, respectively. In Fig. 16a the speed response settling time of PSO-PID is very less compare to Hybrid MOLSA-PID, MOL-PID, GSA-PID, SHO-PID, LUS-PID, RGA-SBX-PID, NSGA-II-PID, respectively. Figure 16b shows the No-load torque at 2000 rpm, here PSO-PID has very less torque ripples compare to MOLSA-PID, MOL-PID, GSA-PID, SHO-PID, LUS-PID, RGA-SBX-PID, NSGA-II-PID.

Case 2: load torque T = 50Nm. At a load of 50N.m, the speed response settling time of PSO-FOPID lower when compared to previous optimization techniques is shown in Fig. 17d. The speed response settling time of LUS-FOPID high compare to other optimization algorithms. Figure 17c shows the speed response at different optimization algorithms using FOPID controller, here PSO-FOPID. Figure 17a shows the speed response of different optimization techniques with PID controller. PSO-PID faster speed response then compare to other techniques. Figure 17b shows the 50N.m load torque of PID controller using Different optimization algorithms and torque ripples of PSO-PID has less compare to other Techniques. If we compare

PSO-FOPID with PSO-PID, PSO-FOPID has less torque ripples and faster speed response.

Case 3: load torque T = 100Nm. The Simulation results for different optimization algorithm with FOPID and PID controller case are shown in Fig. 18. PSO-FOPID technique, as illustrated in Fig. 18c, significantly improves the speed response of SRM and speed settling time, compared to the PSO-PID controller shown in Fig. 18a and other optimization strategies in this study, the PSO-FOPID controller delivers a very quick speed response. Figure 18b, d shows the 100N.m load torque at different optimization techniques using PID and FOPID controllers, here PSO-FOPID gives less torque ripples compare to PSO- PID and other optimization techniques.

The best FF for each of the three scenarios is shown in the Tables 3, 4, 5, 6, 7, 8 utilizing various optimization techniques with PID and FOPID controller methods. When compared to other optimization strategies, it can be seen that the PSO-PID and PSO-FOPID controllers have the lowest FF. PSO-FOPID controller is superior to PSO-PID in terms of optimal values, settling time, speed response time, and torque ripples.

6 Conclusions

To control the speed of an SRM motor and minimize the integral square error (ISE) of speed, current, and torque ripples, this work proposes a cascaded FOPID and PID controller with a particle swarm optimization technique. The optimal gain values for both the speed and current controllers are obtained along the turn-on (T_O), and turn-off (T_F) angles, and the maximum, minimum, mean torque, and torque ripples for various speed and load scenarios are identified. Comparisons with existing optimization methods based on cascaded PID and FOPID controllers, such as the SHO, LUS, GA, Ant-Lion, NSGA-II, MOLGSA, GSA, Hybrid MOLGSA, and RGA-SBX algorithms, show that a cascaded fractional order PID controller offers better speed, current, and torque responses, as well as smaller current and torque ripples, under numerous different types of load and speed conditions. Under all load conditions, it has been demonstrated that the PSO-FOPID controller has the best speed response and minimal torque ripples when compared to the PSO-PID controller. Based on the research results, it is possible to conclude that PSO-FOPID-based speed controllers increase SRM drive performance by minimizing torque ripple and settling time and giving a superior current profile due to their high exploitation capacity.

6.1 Future scope

Hardware Implementation of Switched reluctance motor can be done and compared simulation results with hardware results.

Appendix

SRM Drive Parameters	Ratings
Power	60KW
Voltage	240Volts
stator pole arc	30Deg
rotor pole arc	32Deg
stack length	51 mm
stator diameter	82.1 mm
rotor diameter	40 mm
number of windings per pole	72 turns
stator resistance	0.05Ω
inertia	0.05 kg.m2
friction	0.02 N.m.s
No of rotor poles	4
No of stator poles	6

References

1. Harris MR, Miller THE (1989) Comparison of design and performance parameters in switched reluctance and induction motors. In: Fourth international conference on electrical machines and drives. IET, pp 303–307
2. Ye J, Bilgin B, Emadi A (2015) An offline torque sharing function for torque ripple reduction in switched reluctance motor drives. IEEE Trans Energy Convers 30(2):726–735. https://doi.org/10.1109/TEC.2014.2383991
3. Wu W, Lovatt HC, Dunlop JB (2002) Optimisation of switched reluctance motors for hybrid electric vehicles. https://doi.org/10.1049/cp:20020110
4. Barnes M, Pollock C (1998) Power electronic converters for switched reluctance drives. IEEE Trans Power Electron 13(6):1100–1111. https://doi.org/10.1201/9780203729991-10
5. Gan C, Wu J, Sun Q, Kong W, Li H, Hu Y (2018) A review on machine topologies and control techniques for low-noise switched reluctance motors in electric vehicle applications. IEEE Access 6:31430–31443. https://doi.org/10.1109/ACCESS.2018.2837111
6. Rezig A, Boudendouna W, Djerdir A, N'Diaye A (2020) Investigation of optimal control for vibration and noise reduction in-wheel switched reluctance motor used in electric vehicle. Math Comput Simul 167:267–280. https://doi.org/10.1016/j.matcom.2019.05.016
7. Labiod C, Srairi K, Mahdad B, Benchouia MT, Benbouzid M (2015) Speed control of 8/6 switched reluctance motor with torque ripple reduction taking into account magnetic saturation effects. Energy Procedia 74:112–121. https://doi.org/10.1016/j.egypro.2015.07.530
8. Maksoud HA (2020) Torque ripple minimization of a switched reluctance motor using a torque sharing function based on the overlap control technique. Eng Technol Appl Sci Res 10(2):5371–5376. https://doi.org/10.48084/etasr.3389

9. Abdel-Fadil R, Számel L (2020) Predictive direct torque control of switched reluctance motor for electric vehicles drives. Periodica Polytechnica Electr Eng Comput Sci 64(3):264–273. https://doi.org/10.3311/PPee.15496

10. Jamil MU, Kongprawechnon W, Chayopitak N (2017) Average torque control of a switched reluctance motor drive for light electric vehicle applications. IFAC-PapersOnLine 50(1):11535–11540. https://doi.org/10.1016/j.ifacol.2017.08.1628

11. Hamouda M, Menaem AA, Rezk H, Ibrahim MN, Számel L (2020) Numerical estimation of switched reluctance motor excitation parameters based on a simplified structure average torque control strategy for electric vehicles. Mathematics 8:1213. https://doi.org/10.3390/math8081213

12. Kotb H, Yakout AH, Attia MA, Turky RA, AboRas KM (2022) Speed control and torque ripple minimization of SRM using local unimodal sampling and spotted hyena algorithms based cascaded PID controller. Ain Shams Eng J 13(4):101719. https://doi.org/10.1016/j.asej.2022.101719

13. Saha N, Panda S (2017) Speed control with torque ripple reduction of switched reluctance motor by hybrid many optimizing liaison gravitational search technique. Eng Sci Technol Int J 20(3):909–921. https://doi.org/10.1016/j.jesit.2016.12.013

14. Prasad ES, and Sanker Ram BV (2016) Ant-lion optimizer algorithm based FOPID controller for speed control and torque ripple minimization of SRM drive system. In: International conference on signal processing, communication, power and embedded system. https://doi.org/10.1109/SCOPES.2016.7955700

15. Kumar MN, Chidanandappa R (2022) Novel design and simulation of fuzzy controller for turn-on & turn-off angle in coordination with SRM speed control for electric vehicles. Indones J Electr Eng Inf (IJEEI) 10(2):246–262. https://doi.org/10.52549/ijeei.v10i2.3700

16. Manjula A, Kalaivani L, Gengaraj M, Maheswari RV, Vimal S, Kadry S (2021) Performance enhancement of SRM using smart bacterial foraging optimization algorithm-based speed and current PID controllers. Comput Electr Eng 95:107398. https://doi.org/10.1016/j.compeleceng.2021.107398

17. Ibrahim HE-SA, Mohamed Said SA, Khaled Mohamed A (2018) Speed control of switched reluctance motor using genetic algorithm and ant colony based on optimizing PID controller. In ITM Web of Conferences, vol 16. EDP Sciences, p 01001. https://doi.org/10.1051/itmconf/20181601001

18. Nimisha KK, and Senthilkumar R. Optimal tuning of PID controller for switched reluctance motor speed control using particle swarm optimization. In: International conference on control, power, communication and computing technologies (ICCPCCT). IEEE, pp 487–491. https://doi.org/10.1109/ICCPCCT.2018.8574234

19. Prasad ES, Sanker Ram BV (2016) Multi-objective optimized controller for torque ripple minimization of switched reluctance motor drive system. Indian J Sci Technol 9(20):1–10. https://doi.org/10.17485/ijst/2016/v9i20/91308

20. Lan Y, Benomar Y, Deepak K, Aksoz A, El Baghdadi M, Bostanci E, Hegazy O (2021) Switched reluctance motors and drive systems for electric vehicle powertrains: State of the art analysis and future trends. Energies 14(8):2079. https://doi.org/10.3390/en14082079

21. Gao X, Na R, Jia C, Wang X, Zhou Y (2018) Multi-objective optimization of switched reluctance motor drive in electric vehicles. Comput Electr Eng 70:914–930. https://doi.org/10.1016/j.compeleceng.2017.12.016

22. Gengaraj M, Kalaivani L, Rajesh R (2023) Investigation on torque sharing function for torque ripple minimization of switched reluctance motor: a flower pollination algorithm based approach. IETE J Res 69:3678–3692. https://doi.org/10.1080/03772063.2022.2112312

23. Oshaba AS, Ali ES, Abd Elazim SM (2015) ACO based speed control of SRM fed by photovoltaic system. Int J Electr Power Energy Syst 67:529–536. https://doi.org/10.1016/j.ijepes.2014.12.009

24. Hamouda M, Menaem AA, Rezk H, Ibrahim MN, Számel L (2021) Comparative evaluation for an improved direct instantaneous torque control strategy of switched reluctance motor drives for electric vehicles. Mathematics 9:302. https://doi.org/10.3390/math9040302

25. RGhoudelbourk, Sihem, Ahmad Taher Azar, Djalel D, Abelkrim R (2022) Fractional order control of switched reluctance motor. Int J Adv Intell Paradigms 21(3–4):247–266. https://doi.org/10.1504/IJAIP.2022.122191

26. El-Hay EA, El-Hameed MA, El-Fergany AA (2019) Improved performance of PEM fuel cells stack feeding switched reluctance motor using multi-objective dragonfly optimizer. Neural Comput Appl 31:6909–6924. https://doi.org/10.1007/s00521-018-3524-z

27. Kalaivani L, Subburaj P, Willjuice Iruthayarajan M (2013) Speed control of switched reluctance motor with torque ripple reduction using non-dominated sorting genetic algorithm (NSGA-II). Int J Electr Power Energy Syst 53:69–77. https://doi.org/10.1016/j.ijepes.2013.04.005

28. Rodrigues M, Costa Branco PJ, Suemitsu W (2001) Fuzzy logic torque ripple reduction by turn-off angle compensation for switched reluctance motors. IEEE Trans Ind Electron 48(3):711–715. https://doi.org/10.1109/41.925598

29. Saha N, Panda AK, Panda S (2018) Speed control with torque ripple reduction of switched reluctance motor by many optimizing liaison techniques. J Electr Syst Inf Technol 5(3):829–842. https://doi.org/10.1016/j.jesit.2016.12.013

30. Chichate KR, Gore SR and Zadey A (2020) Modelling and simulation of switched reluctance motor for speed control applications. 2020 2nd international conference on innovative mechanisms for industry applications (ICIMIA), Bangalore, India, 2020, pp. 637–640, doi: https://doi.org/10.1109/ICIMIA48430.2020.9074845.

31. Tariq I, Muzzammel R, Alqasmi U, Raza A (2020) Artificial neural network-based control of switched reluctance motor for torque ripple reduction. Math Probl Eng 2020:1–31. https://doi.org/10.1155/2020/9812715

32. Khan H, Khatoon S, Gaur P (2021) Comparison of various controller design for the speed control of DC motors used in two wheeled mobile robots. Int j inf tecnol 13:713–720. https://doi.org/10.1007/s41870-020-00577-8

33. Deshmukh RA, Hasamnis MA (2023) An improvement to the conventional PD scheme for the speed control of a two-wheeled differential steering mobile robot. Int j inf tecnol 15:3093–3101. https://doi.org/10.1007/s41870-023-01337-0

34. Krishnan R (2017) Switched reluctance motor drives: modeling, simulation, analysis, design, and applications. CRC Press. https://doi.org/10.1201/9781420041644

35. Kanwar K, Vajpai J, Meena SK (2022) Design of PSO tuned PID controller for different types of plants. Int j inf tecnol 14:2877–2884. https://doi.org/10.1007/s41870-022-01051-3

36. Madhusudhan M, Pradeepa H, Jayasankar VN (2023) Grey wolf optimization based fractional order PID controller in SSSC on damping low frequency oscillation in interconnected multi-machine power system. Int j inf tecnol. https://doi.org/10.1007/s41870-023-01253-3

37. Pathak D, Gaur P (2021) Output power control of wind energy system by tip speed ratio control using fractional $PI^{\beta}D^{\alpha}$ controller. Int j inf tecnol 13:299–305. https://doi.org/10.1007/s41870-020-00519-4